PHYSICAL REVIEW C **104**, L042801 (2021)

Letter

First direct measurement of ^{59}Cu$(p,\alpha)^{56}$Ni: A step towards constraining the Ni-Cu cycle in the cosmos

J. S. Randhawa[1,*] R. Kanungo,[2,3,†] J. Refsgaard,[2,3] P. Mohr,[4] T. Ahn,[1] M. Alcorta,[3] C. Andreoiu,[5] S. S. Bhattacharjee,[2,3,6] B. Davids,[3,7] G. Christian,[2] A. A. Chen,[8] R. Coleman,[9] P. E. Garrett,[9] G. F. Grinyer,[10] E. Gyabeng Fuakye,[10] G. Hackman,[3] J. Hollett,[2] R. Jain,[11] K. Kapoor,[10] R. Krücken,[3,12] A. Laffoley,[9] A. Lennarz,[3,8] J. Liang,[8] Z. Meisel,[13] B. Nikhil,[2] A. Psaltis,[14] A. Radich,[9] M. Rocchini,[9] N. Saei,[10] M. Saxena,[13] M. Singh,[2] C. Svensson,[9] P. Subramaniam,[2] A. Talebitaher,[10] S. Upadhyayula,[3] C. Waterfield,[2] J. Williams,[3] and M. Williams[3]

[1]Department of Physics and Joint Institute for Nuclear Astrophysics, University of Notre Dame, Notre Dame, Indiana 46556, USA
[2]Astronomy and Physics Department, Saint Mary's University, Halifax, Nova Scotia B3H 3C3, Canada
[3]TRIUMF, Vancouver, British Columbia V6T 2A3, Canada
[4]Institute for Nuclear Research (Atomki), P.O. Box 51, Debrecen H-4001, Hungary
[5]Department of Chemistry, Simon Fraser University, Burnaby, British Columbia V5A 1S6, Canada
[6]Institute of Experimental and Applied Physics, Czech Technical University in Prague, Husova 240/5, 110 00 Prague 1, Czech Republic
[7]Department of Physics, Simon Fraser University, Burnaby, British Columbia V5A 1S6, Canada
[8]Department of Physics and Astronomy, McMaster University, Hamilton, Ontario L8S 4M1, Canada
[9]Department of Physics, University of Guelph, Guelph, Ontario N1G 2W1, Canada
[10]Department of Physics, University of Regina, Regina, Saskatchewan S4S 0A2, Canada
[11]Facility for Rare Isotope Beams, Michigan 48824, USA
[12]Department of Physics and Astronomy, University of British Columbia, Vancouver, British Columbia V6T 1Z1, Canada
[13]Institute of Nuclear and Particle Physics, Department of Physics & Astronomy, Ohio University, Athens, Ohio 45701, USA
[14]Institut für Kernphysik, Technische Universität Darmstadt, D-64289 Darmstadt, Schlossgartenstraße 2, Germany

(Received 12 July 2021; accepted 6 October 2021; published 28 October 2021)

Reactions on proton-rich nuclides drive the nucleosynthesis in core collapse supernovae (CCSNe) and in x-ray bursts (XRBs). CCSNe eject the nucleosynthesis products to the interstellar medium and hence are a potential inventory of p nuclei, whereas in XRBs nucleosynthesis powers the light curves. In both astrophysical sites the Ni-Cu cycle, which features a competition between ^{59}Cu$(p,\alpha)^{56}$Ni and ^{59}Cu$(p,\gamma)^{60}$Zn, could potentially halt the production of heavier elements. Here, we report the first direct measurement of ^{59}Cu$(p,\alpha)^{56}$Ni using a reaccelerated ^{59}Cu beam and a cryogenic solid hydrogen target. Our results show that the reaction proceeds predominantly to the ground state of ^{56}Ni, and the experimental rate has been found to be lower than Hauser-Feshbach based statistical model predictions. New results hints that the νp process could operate at higher temperatures than previously inferred and therefore remains a viable site for synthesizing the heavier elements.

DOI: 10.1103/PhysRevC.104.L042801

In the Universe most of the heavy elements not made in the slow neutron capture in stellar burning are produced via rapid neutron capture (r process) proposed to occur in neutron star mergers (NSMs) [1,2]. The recent discovery of gravitational waves from NSMs and followup multiwavelength observations have bolstered the NSMs as a viable site for heavy elements synthesis [2]. However, there are several nuclides (≈30 nuclides of 23 elements) that cannot be synthesized in the r process or s process. Especially, the mechanism for the production of the light p nuclei, ^{92,94}Mo and ^{96,98}Ru, is still debatable [3–5]. Nucleosynthesis on the proton-rich side, e.g., the νp process in core-collapse supernovae (CCSNe) and the rp process in type-I x-ray bursts (XRBs) has been suggested as sites where these p nuclei can be synthesized [6–8].

In both the rp process and νp process, as soon as the reaction flow reaches ^{59}Cu, the ^{59}Cu(p,α) and ^{59}Cu(p,γ) reactions start competing due to the lower α-emission threshold in ^{60}Zn compared to the proton threshold. This leads to the Ni-Cu cycle occurring in two different astrophysical sites, i.e., in the x-ray bursts (rp process) and in CCSNe (νp process) [9–11]. ^{59}Cu$(p,\alpha)^{56}$Ni returns the cycle to ^{56}Ni, while ^{59}Cu(p,γ) breaks out of the Ni-Cu cycle and takes the flow further, depending on the $(p,\gamma)/(p,\alpha)$ rate ratio. In the case of the νp process, if ^{59}Cu$(p,\alpha)^{56}$Ni is dominating over (p,γ) over the wide range of relevant temperatures, there is little flow above ^{59}Cu and hence the νp process cannot be a contender for the synthesis of heavier p nuclei. As for the rp process, the ashes of XRBs do not become part of the interstellar medium and they are therefore an unlikely source of heavy nuclei. Instead, they are buried deeper in the neutron star, which plays an important role in determining the thermal profile of the neutron star crust. However, the Ni-Cu cycle significantly affects the

*jrandhaw@nd.edu
†ritu@triumf.ca

energy generation and hence the shape of XRB light curves. Hence ^{59}Cu$(p,\alpha)^{56}$Ni is one of the few identified reactions which directly impacts the XRB light curves and hinders the XRB light curve model-observation comparison [11]. Therefore, it is of foremost importance to measure ^{59}Cu$(p,\alpha)^{56}$Ni in addition to ^{59}Cu$(p,\gamma)^{60}$Zn to understand the Ni-Cu cycle in the νp process and in XRBs.

In this work, we focus on the ^{59}Cu$(p,\alpha)^{56}$Ni reaction. Currently, there is no experimental information on this reaction rate. The relevant temperature ranges for XRBs and the νp process are ≈1 GK and 1–4 GK, respectively. The corresponding Gamow window is 1.1–1.4 MeV for XRBs and 1.1 to 4.04 MeV for the νp process. Direct measurement of ^{59}Cu$(p,\alpha)^{56}$Ni in the Gamow window is an arduous task because the predicted cross sections are very small and production of a high intensity radioactive ^{59}Cu beam is very challenging. Therefore, in an alternative approach there have been attempts to measure the time-inverse reaction cross sections, i.e., ^{56}Ni$(\alpha,p)^{59}$Cu [12]. However, these time-inverse measurements are valid if ^{59}Cu$(p,\alpha)^{56}$Ni exclusively proceeds to the ground state of ^{56}Ni. Current estimates of ^{59}Cu$(p,\alpha)^{56}$Ni and time-inverse ^{56}Ni(α,p) are based on the Hauser-Feshbach based statistical model codes. Hauser-Feshbach based models are expected to provide reliable predictions for the reactions where the nuclear level density in the compound nucleus is high enough to apply statistical models [13]. However, a few recent experiments including ^{33}Cl$(p,\alpha)^{30}$S [14] and ^{34}Ar$(\alpha,p)^{37}$K [15], have provided the first hints of large discrepancies (more than a factor of 10) between experimental data and predicted (p,α) and (α,p) reaction rates on neutron deficient nuclei, even though the nuclear level densities are high enough to apply the statistical models. Various studies have shown that, even though other parameters could be a source of uncertainty too, α optical model potentials (α-OMPs) remained an important source of uncertainty in the Hauser-Feshbach based statistical model calculations. It has been shown by Gyürky *et al.* [16], where they focused on ^{64}Zn$(p,\alpha)^{61}$Cu reaction, that (p,α) cross sections in the $A = 60$ mass region depend essentially on the chosen α-OMP. Moreover, in the work of Avrigeanu and Avrigeanu [17], it was shown that the α optical model potentials (α-OMPs) which reproduce the α-induced reaction data lead to the underestimated predictions of the statistical models for the (n,α) reaction cross sections. As the above-mentioned cases have a level density in the compound nucleus similar to that known for ^{60}Zn [18], the validity of statistical models needs to be ascertained against a direct measurement of the ^{59}Cu$(p,\alpha)^{56}$Ni reaction cross section. Therefore, it is important to perform a direct measurement of ^{59}Cu$(p,\alpha)^{56}$Ni at energies above the Gamow window where cross sections are higher. The results can be used to test the validity of the Hauser-Feshbach approach commonly used to predict the stellar ^{59}Cu(p,α) rate and its inverse, i.e., ^{56}Ni(α,p)^{59}Cu, and to constrain Hauser-Feshbach model parameters.

We report the first direct measurement of ^{59}Cu$(p,\alpha)^{56}$Ni using the IRIS facility with a cryogenic solid H_2 target and a reaccelerated ^{59}Cu beam at TRIUMF. We provide the total cross sections at a center-of-mass energy $E_{c.m.} = 6.0$ MeV and demonstrate that a significant contribution comes from populating the ground state of ^{56}Ni.

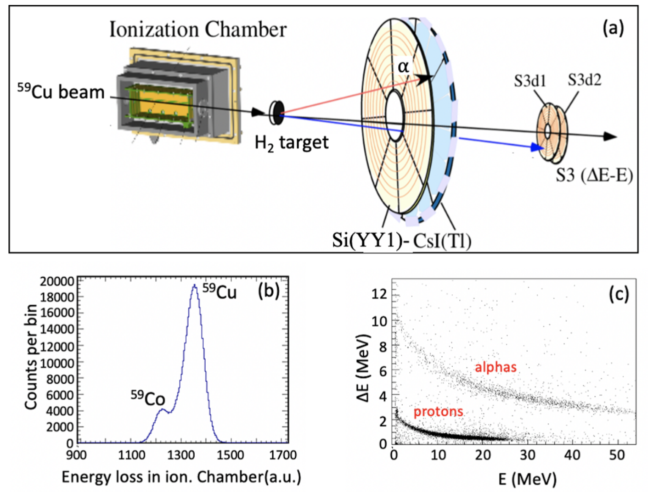

FIG. 1. The upper panel shows the schematic of IRIS set-up which includes an ionization chamber followed by a solid H_2 target and two ΔE-E telescopes for particle identification. The bottom left panel shows the energy loss spectrum of beam particles in the ionization chamber and the bottom right panel shows the particle identification using the Si(YY1)-CsI(Tl) ΔE-E telescope.

Experiment details. The experiment was performed using IRIS facility in ISAC-II at TRIUMF. A schematic of the detector layout of IRIS is shown in Fig. 1; for more details please see Ref. [19]. The radioactive beam of ^{59}Cu was produced via spallation of a niobium target with 480 MeV protons. The ^{59}Cu beam was re-accelerated using the ISAC-II superconducting LINAC to 8.5*A* MeV and then passed through an ionization chamber, filled with isobutane gas at 19.5 Torr at room temperature. The average beam intensity was ≈3600 pps. The energy loss of the beam measured in this ionization chamber provided an event-by-event identification of the ^{59}Cu incident beam and its contaminant ^{59}Co throughout the experiment. Following this, the beam interacts with a thin windowless solid hydrogen (H_2) reaction target built on a 4.3 μm thick Ag foil backing facing upstream of the H_2 layer. The target cell with the foil was cooled to ≈4 K before forming solid H_2. The solid H_2 target has been been successfully used in various experiments [20–22]. The energy of the elastically scattered beam on the Ag foil was measured with and without H_2, providing continuous measurement of the target thickness during the experiment. These scattered beam particles were detected using a double-sided silicon strip detector placed 52.5 cm downstream of the target, covering laboratory angles of 1.2°–3.8°. The average H_2 target thickness was 53 μm, and the target thickness between the first and last runs of data-taking period showed a change of 7% over the entire data taking period. Protons and α particles from reactions were detected using annular arrays of 100 μm thick single-sided silicon strip detectors followed by a layer of 12 mm thick CsI(Tl) detectors placed 15 cm downstream of the target. This detector combination served as an energy-loss and total energy (E) telescope for identifying the p and α recoils after the target. The CsI(Tl) detectors were calibrated

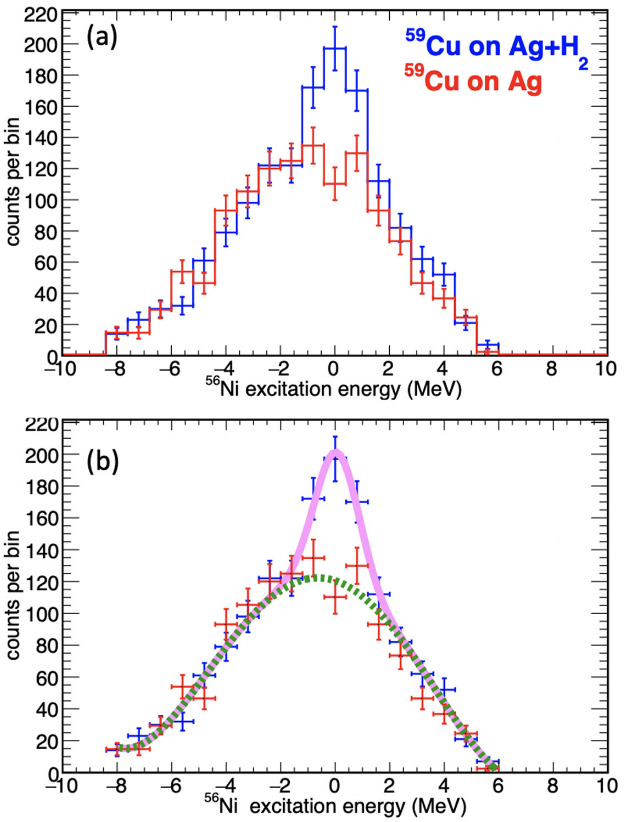

FIG. 2. The upper panel shows the excitation energy spectrum with (blue) and without (red) H_2 target. The lower panel shows the blue histogram fitted with a Gaussian + polynomial function (solid pink line) and the red histogram, i.e., the background fitted with polynomial only (green dotted line).

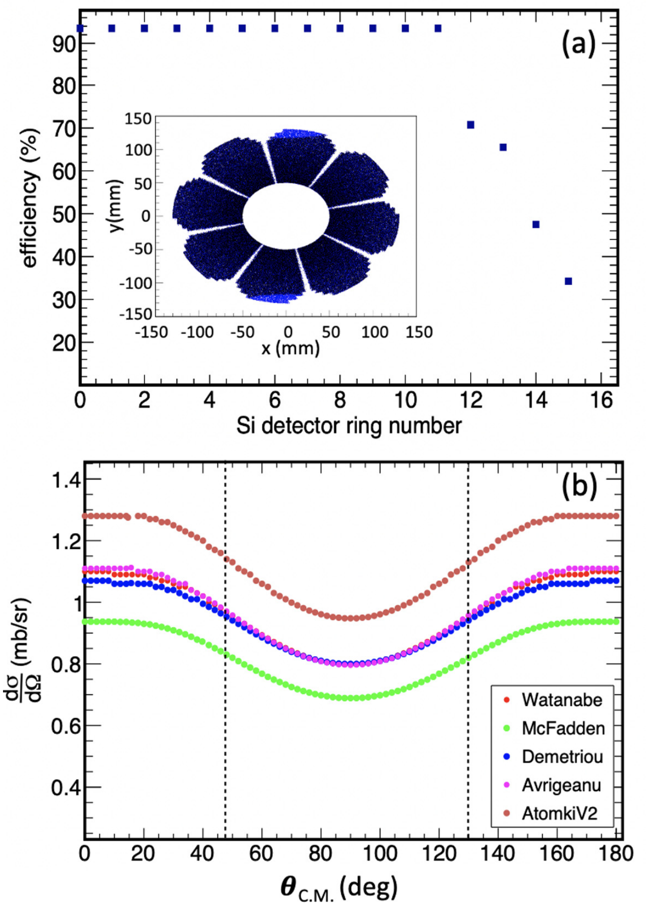

FIG. 3. The upper panel shows the simulated detector efficiency as a function of ring number (which provides the scattering angle). The dark blue in the inset shows the simulated hit pattern. The lower panel shows the calculated angular distributions using different α-OMPs in TALYS. Vertical dotted lines shows the detector coverage.

using ^{59}Cu$(p,p)^{59}$Cu elastic scattering. The detector telescope covered scattering angles of $\theta_{\rm lab} = 18.5^\circ$–$40.7^\circ$.

Results. The excitation energy spectrum of ^{56}Ni, shown in Fig. 2 (upper panel), was reconstructed using the missing mass technique using the energy and scattering angle of the α particles, measured by the silicon-CsI(Tl) (ΔE-E) telescope. The narrow peak centered around ≈0 MeV in the excitation energy spectrum is the ground state of ^{56}Ni. The energy of the first excited state in ^{56}Ni is 2.7 MeV and hence is easily resolved from the ground state in the current experiment. One of the major sources of background is α particles originating from the reactions on the Ag foil. The background from the Ag foil was measured by collecting data without the H_2 target and is shown with a red dashed-dotted histogram (Fig. 2 lower panel) normalized by the incident beam intensity. In this experiment $\theta_{\rm lab} = 18.5^\circ$–$35.5^\circ$, where the lower angle comes from experimental coverage and the higher angle is the maximum allowed angle of α particles at this energy. This corresponds to $\theta_{c.m.} = 48^\circ$–130° when accounting for the experimental acceptance in angle as well as energy. Figure 3 (upper panel) shows the detection efficiency using Monte Carlo simulations. Due to a heat shield surrounding the solid hydrogen target, the efficiency drops at higher angles, and obtained spectra were corrected for this efficiency. The total cross section for ^{59}Cu$(p,\alpha)^{56}$Ni corresponds to integration over $\theta_{c.m.} = 0^\circ$–180°. Since our experimental coverage of $\theta_{c.m.}$ is limited, in order to get angle-integrated counts the angular distribution was calculated using code TALYS [17,23]. Angular distributions obtained using different α optical model potentials (α-OMPs) are shown in Fig. 3 (lower panel). The ratio of integrated cross section in the experimental acceptance to the total cross section provides the correction factor of 0.62 to the experimental results, and variation in this correction factor, using the angular distribution from different potentials, provides an estimate of the systematic uncertainty. The center-of-mass energy ($E_{c.m.}$) at the beginning and the end of the solid H_2 target is 5.7 and 6.3 MeV, respectively. $E_{c.m.}$ at the center of the target corresponds to 6.0 MeV, whereas the weighted energy, defined as $\int \sigma(E)E\,dE / \int \sigma(E)dE$, is 6.02 MeV (where the energy dependence of HF based NON-SMOKER database cross sections was used). Therefore, in this work cross sections are provided at $E_{c.m.} = 6.0$ MeV

From the excitation energy spectrum, a major highlight is that ^{59}Cu$(p,\alpha)^{56}$Ni, within current measurement sensitivity, proceeds exclusively to the ground state of ^{56}Ni. Hence, at the center-of-mass energy $E_{c.m.} = 6.0$ MeV, ^{59}Cu$(p,\alpha)^{56}$Ni$_{g.s}$ is

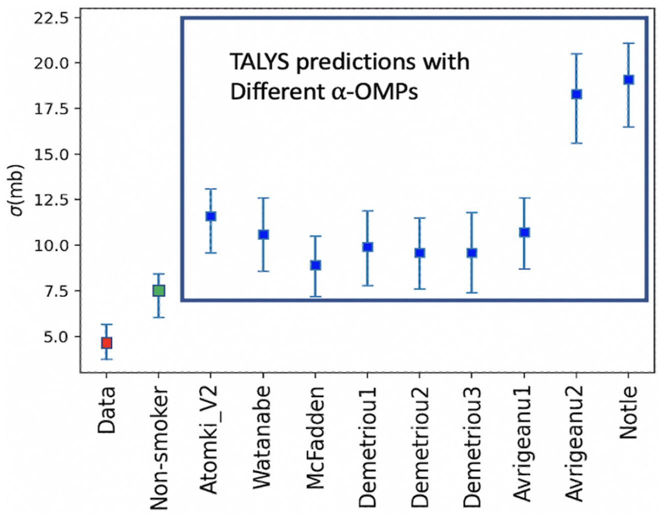

FIG. 4. The cross section obtained in the current work compared to various statistical model calculations at $E_{c.m.} = 6.0$ MeV. Error bars on the calculated cross sections include the total change in the cross sections due to change in the energy inside the target.

equal to the total $^{59}\mathrm{Cu}(p,\alpha)^{56}\mathrm{Ni}$ cross section. The measured cross-section at this energy is shown in Fig. 4 (in the top panel, red square). Experimental error bars reflect both statistical and systematic uncertainties. The systematic uncertainty contains 5% contribution from the beam counts, 5% from target thickness, 15% from angular distribution, and 10% from simulated detection efficiency. Figure 4 (upper panel) shows the comparison of the experimental cross section to statistical model calculations, which includes results from the NON-SMOKER database [24] and TALYS using various input α optical model potentials (α-OMPs) [23,25–29]. Other options used in TALYS calculations are the phenomenological proton OMP and the constant temperature Fermi gas model for level densities (i.e., "ldmodel 1"). Error bars on calculated (theoretical) cross sections reflect the change in cross section across the H_2 target (i.e., we account for total cross section change inside the target). The experimental cross section is lower compared to all the Hauser-Feshbach based statistical model predictions. In general, the (p,α) cross section in the statistical model depends on the transmissions T_i in the entrance and exit channels. Very schematically,

$$\sigma(p,\alpha) \sim \frac{T_{p,0}T_\alpha}{\sum_i T_i}, \tag{1}$$

where at the experimental energy the sum in the denominator is dominated by the elastic and inelastic proton channels. Thus, $\sigma(p,\alpha)$ is essentially sensitive only to the chosen α-OMP whereas other ingredients of the statistical model, like the nucleon OMP, the γ-ray strength function, and the level density, have only marginal influence. Interestingly, all recent α-OMPs predict (p,α) cross sections around 10 mb, thus overestimating the experimental result by about a factor of 2. A somewhat smaller deviation is found for the McFadden-Satchler α-OMP (Fig. 4, top panel).

Impact on νp process and XRBs: In the work of Arcones *et al.* [10], it was shown that that the νp process starts to efficiently produce heavy elements only when the temperature drops below ≈3 GK. At higher temperatures, the reaction $^{59}\mathrm{Cu}(p,\alpha)^{56}\mathrm{Ni}$ is faster than the reaction $^{59}\mathrm{Cu}(p,\gamma)^{60}\mathrm{Zn}$ and hence cycles the reaction flow back to ^{56}Ni. To understand the impact of the measured cross section on the reaction flow in the νp process, one needs to compare the $^{59}\mathrm{Cu}(p,\gamma)^{60}\mathrm{Zn}$ reaction rate with the $^{59}\mathrm{Cu}(p,\alpha)^{56}\mathrm{Ni}$ reaction rate. Currently, these rates are based on the statistical model (in JINA Reaclib [30]). The present measurement shows that statistical models calculations overestimate the (p,α) cross section in this region. Therefore, experimental information on the $^{59}\mathrm{Cu}(p,\gamma)^{60}\mathrm{Zn}$ reaction rate is required to completely understand the impact on the νp process. However, the current study shows that the $^{59}\mathrm{Cu}(p,\alpha)^{56}\mathrm{Ni}$ reaction, a main hindrance in the production of heavier elements in the νp process, is slower than previously predicted. Therefore, a similar deviation of $^{59}\mathrm{Cu}(p,\gamma)^{60}\mathrm{Zn}$ from the statistical model predictions would still uphold the conclusion drawn in Ref. [10]. It supports the νp process as a viable mechanism for the production of ^{92,94}Mo and ^{96,98}Ru p nuclei and other heavier nuclei. A substantial reduction in $^{59}\mathrm{Cu}(p,\gamma)^{60}\mathrm{Zn}$ from the statistical model predictions will be required to completely alter this situation.

However, the situation for XRBs is more complex, where temperatures of interest are 1 GK or below, i.e., lower than that of the νp process. A recent measurement of nuclear level density in ^{60}Zn shows an unexpected plateau at the energies relevant for XRBs [18]. It remains to be seen whether or not the statistical model is valid in the temperature range of XRBs. Therefore, for the XRBs, further measurements are required to understand the contribution of individual resonances to both $^{59}\mathrm{Cu}(p,\alpha)^{56}\mathrm{Ni}$ and $^{59}\mathrm{Cu}(p,\gamma)^{60}\mathrm{Zn}$ reaction rates. The current experiment shows that $^{59}\mathrm{Cu}(p,\alpha)^{56}\mathrm{Ni}$ predominantly proceeds to the ground state of ^{56}Ni; therefore, measurement of the time-inverse reaction, i.e., $^{56}\mathrm{Ni}(\alpha,p)^{59}\mathrm{Cu}$, could be a viable option too as more intense ^{56}Ni beams are possible compared to the challenging production of a ^{59}Cu beam. Nonetheless, either direct or time-inverse measurements are required in the XRB Gamow window to infer the applicability of statistical models and will help elucidate the role of the Ni-Cu cycle in XRBs.

To summarize, we report the first direct measurement of the $^{59}\mathrm{Cu}(p,\alpha)^{56}\mathrm{Ni}$ reaction cross section using a pure solid H_2 target at the IRIS facility at TRIUMF. The new measurement shows that $^{59}\mathrm{Cu}(p,\alpha)^{56}\mathrm{Ni}$ proceeds predominantly to the ground state of ^{56}Ni. The new cross section is a factor of 1.6 to 4 lower compared to commonly used statistical model predictions. A slower $^{59}\mathrm{Cu}(p,\alpha)^{56}\mathrm{Ni}$ reaction, compared to that previously used in the calculations, hints that the Ni-Cu cycle in the νp process might not hinder the production of heavier elements. However, future measurements to constrain the $^{59}\mathrm{Cu}(p,\gamma)^{60}\mathrm{Zn}$ reaction rate would be required to further elucidate the flow in the Ni-Cu cycle.

We would like to acknowledge the support of the beam delivery group at TRIUMF. J.S.R. thanks A. Simon for useful discussions. J.S.R. and T.A. were supported by NSF Grant No. 2011890. Support from NSERC, CFI, and Research

Nova Scotia is gratefully acknowledged. Z.M. is supported by the U.S. Department of Energy, Office of Science, Grants No. DE-FG02-88ER40387 and No. DE-SC0019042. TRIUMF receives funding via a contribution through the National Research Council Canada. The support from RCNP for the target is gratefully acknowledged. It was partly supported by the grant-in-aid program of the Japanese government under the Contracts No. 23224008 and No. 14J03935.

[1] D. Kasen, B. Metzger, J. Barnes, E. Quataert, and E. Ramirez-Ruiz, Origin of the heavy elements in binary neutron-star mergers from a gravitational-wave event, Nature (London) **551**, 80 (2017).
[2] S. J. Smartt, T.-W. Chen, A. Jerkstrand *et al.*, A kilonova as the electromagnetic counterpart to a gravitational-wave source, Nature (London) **551**, 75 (2017).
[3] J. Bliss, A. Arcones, and Y.-Z. Qian, Production of Mo and Ru isotopes in neutrino-driven winds: Implications for solar abundances and presolar grains, Astrophys. J. **866**, 105 (2018).
[4] B. S. Meyer, The r-, s-, and p-processes in nucleosynthesis, Annu. Rev. Astron. Astrophys. **32**, 153 (1994).
[5] S. Goriely, A. Bauswein, and H.-T. Janka, r-process nucleosynthesis in dynamically ejected matter of neutron star mergers, Astrophys. J. **738**, L32 (2011).
[6] C. Fröhlich, G. Martínez-Pinedo, M. Liebendörfer, F.-K. Thielemann, E. Bravo, W. R. Hix, K. Langanke, and N. T. Zinner, Neutrino-Induced Nucleosynthesis of $A > 64$ Nuclei: The νp Process, Phys. Rev. Lett. **96**, 142502 (2006).
[7] A. Arcones and F. Montes, Production of light-element primary process nuclei in neutrino-driven winds, Astrophys. J. **731**, 5 (2011).
[8] H. Schatz, A. Aprahamian, V. Barnard, L. Bildsten, A. Cumming, M. Ouellette, T. Rauscher, F.-K. Thielemann, and M. Wiescher, End Point of the *rp* Process on Accreting Neutron Stars, Phys. Rev. Lett. **86**, 3471 (2001).
[9] L. van Wormer, J. Görres, C. Iliadis, M. Wiescher, and F. K. Thielemann, Reaction rates and reaction sequences in the rp-process, Astrophys. J. **432**, 326 (1994).
[10] A. Arcones, C. Fröhlich, and G. Martinez-Pinedo, Impact of supernova dynamics on the νp-process, Astrophys. J. **750**, 18 (2012).
[11] R. H. Cyburt, A. M. Amthor, A. Heger, E. Johnson, L. Keek, Z. Meisel, H. Schatz, and K. Smith, Dependence of x-ray burst models on nuclear reaction rates, Astrophys. J. **830**, 55 (2016).
[12] K. Schmidt, ^{56}Ni(α, p) cross-section measurement, National Superconducting Cyclotron Laboratory Proposal No. 18039, 2016.
[13] T. Rauscher, F.-K. Thielemann, and K.-L. Kratz, Nuclear level density and the determination of thermonuclear rates for astrophysics, Phys. Rev. C **56**, 1613 (1997).
[14] C. M. Deibel, K. E. Rehm, J. M. Figueira, J. P. Greene, C. L. Jiang, B. P. Kay, H. Y. Lee, J. C. Lighthall, S. T. Marley, R. C. Pardo, N. Patel, M. Paul, C. Ugalde, A. Woodard, A. H. Wuosmaa, and G. Zinkann, First measurement of the ^{33}Cl$(p, \alpha)^{30}$S reaction, Phys. Rev. C **84**, 045802 (2011).
[15] A. M. Long, T. Adachi, M. Beard, G. P. A. Berg, Z. Buthelezi, J. Carter, M. Couder, R. J. deBoer, R. W. Fearick, S. V. Förtsch, J. Görres, J. P. Mira, S. H. T. Murray, R. Neveling, P. Papka, F. D. Smit, E. Sideras-Haddad, J. A. Swartz, R. Talwar, I. T. Usman *et al.*, Indirect study of the stellar ^{34}Ar$(\alpha, p)^{37}$K reaction rate through ^{40}Ca$(p, t)^{38}$Ca reaction measurements, Phys. Rev. C **95**, 055803 (2017).
[16] G. Gyürky, Z. Fülöp, Z. Halász, G. G. Kiss, and T. Szücs, Direct study of the α-nucleus optical potential at astrophysical energies using the ^{64}Zn$(p, \alpha)^{61}$Cu reaction, Phys. Rev. C **90**, 052801 (2014).
[17] V. Avrigeanu and M. Avrigeanu, Consistent optical potential for incident and emitted low-energy α particles. ii. α emission in fast-neutron-induced reactions on Zr isotopes, Phys. Rev. C **96**, 044610 (2017).
[18] D. Soltesz, M. A. A. Mamun, A. V. Voinov, Z. Meisel, B. A. Brown, C. R. Brune, S. M. Grimes, H. Hadizadeh, M. Hornish, T. N. Massey, J. E. O'Donnell, and W. E. Ormand, Determination of the ^{60}Zn level density from neutron evaporation spectra, Phys. Rev. C **103**, 015802 (2021).
[19] R. Kanungo, Iris: The ISAC charged particle reaction spectroscopy facility for reaccelerated high-energy ISOL beams, in *ISAC and ARIEL: The TRIUMF Radioactive Beam Facilities and the Scientific Program*, edited by J. Dilling, R. Krücken, and L. Merminga (Springer Netherlands, Dordrecht, 2014), pp. 235–240.
[20] R. Kanungo, A. Sanetullaev, J. Tanaka, S. Ishimoto, G. Hagen, T. Myo, T. Suzuki, C. Andreoiu, P. Bender, A. A. Chen, B. Davids, J. Fallis, J. P. Fortin, N. Galinski, A. T. Gallant, P. E. Garrett, G. Hackman, B. Hadinia, G. Jansen, M. Keefe *et al.*, Evidence of Soft Dipole Resonance in ^{11}Li with Isoscalar Character, Phys. Rev. Lett. **114**, 192502 (2015).
[21] A. Kumar, R. Kanungo, A. Calci, P. Navrátil, A. Sanetullaev, M. Alcorta, V. Bildstein, G. Christian, B. Davids, J. Dohet-Eraly, J. Fallis, A. T. Gallant, G. Hackman, B. Hadinia, G. Hupin, S. Ishimoto, R. Krücken, A. T. Laffoley, J. Lighthall, D. Miller *et al.*, Nuclear Force Imprints Revealed on the Elastic Scattering of Protons with ^{10}C, Phys. Rev. Lett. **118**, 262502 (2017).
[22] J. S. Randhawa, R. Kanungo, M. Holl, J. D. Holt, P. Navrátil, S. R. Stroberg, G. Hagen, G. R. Jansen, M. Alcorta, C. Andreoiu, C. Barnes, C. Burbadge, D. Burke, A. A. Chen, A. Chester, G. Christian, S. Cruz, B. Davids, J. Even, G. Hackman *et al.*, Observation of excited states in ^{20}Mg sheds light on nuclear forces and shell evolution, Phys. Rev. C **99**, 021301 (2019).
[23] P. Demetriou, C. Grama, and S. Goriely, Improved global α-optical model potentials at low energies, Nucl. Phys. A **707**, 253 (2002).
[24] T. Rauscher and F.-K. Thielemann, Astrophysical reaction rates from statistical model calculations, At. Data Nucl. Data Tables **75**, 1 (2000).
[25] L. McFadden and G. Satchler, Optical-model analysis of the scattering of 24.7 MeV alpha particles, Nucl. Phys. **84**, 177 (1966).
[26] V. Avrigeanu, M. Avrigeanu, and C. Mănăilescu, Further explorations of the α-particle optical model potential at low energies for the mass range $a \approx 45$–209, Phys. Rev. C **90**, 044612 (2014).

[27] V. Avrigeanu, P. E. Hodgson, and M. Avrigeanu, Global optical potentials for emitted alpha particles, Phys. Rev. C **49**, 2136 (1994).

[28] M. Nolte, H. Machner, and J. Bojowald, Global optical potential for α particles with energies above 80 MeV, Phys. Rev. C **36**, 1312 (1987).

[29] P. Mohr, Z. Fülöp, G. Gyürky, G. G. Kiss, and T. Szücs, Successful Prediction of Total α-Induced Reaction Cross Sections at Astrophysically Relevant Sub-Coulomb Energies Using a Novel Approach, Phys. Rev. Lett. **124**, 252701 (2020).

[30] R. H. Cyburt, A. M. Amthor, R. Ferguson, Z. Meisel, K. Smith, S. Warren, A. Heger, R. D. Hoffman, T. Rauscher, A. Sakharuk, H. Schatz, F. K. Thielemann, and M. Wiescher, The JINA Reaclib database: Its recent updates and impact on type-I x-ray bursts, Astrophys. J. Suppl. Ser. **189**, 240 (2010).